Published in final edited form as:

*Nanotoxicology*. 2014 September ; 8(6): 663–675. doi:10.3109/17435390.2013.822115.

# Iron oxide nanoparticle agglomeration influences dose rates and modulates oxidative stress-mediated dose–response profiles *in vitro*

**Gaurav Sharma**[1,2,4], **Vamsi Kodali**[2], **Matthew Gaffrey**[2], **Wei Wang**[3,4], **Kevin R. Minard**[2,4], **Norman J. Karin**[2,4], **Justin G. Teeguarden**[2,4], and **Brian D. Thrall**[2,4]

[1]Battelle Memorial Institute, Columbus, OH, USA

[2]Biological Sciences Division, Center for Nanotoxicology, Pacific Northwest National Laboratory, Richland, WA, USA

[3]Environmental Science Division, Oak Ridge National Laboratory, Oak Ridge, TN, USA

[4]Battelle Center for Fundamental and Applied Systems Toxicology, Richland, WA, USA

## Abstract

Spontaneous agglomeration of engineered nanoparticles (ENPs) is a common problem in cell culture media which can confound interpretation of *in vitro* nanotoxicity studies. The authors created stable agglomerates of iron oxide nanoparticles (IONPs) in conventional culture medium, which varied in hydrodynamic size (276 nm–1.5 μm) but were composed of identical primary particles with similar surface potentials and protein coatings. Studies using C10 lung epithelial cells show that the dose rate effects of agglomeration can be substantial, varying by over an order of magnitude difference in cellular dose in some cases. Quantification by magnetic particle detection showed that small agglomerates of carboxylated IONPs induced greater cytotoxicity and redox-regulated gene expression when compared with large agglomerates on an equivalent total cellular IONP mass dose basis, whereas agglomerates of amine-modified IONPs failed to induce cytotoxicity or redox-regulated gene expression despite delivery of similar cellular doses. Dosimetry modelling and experimental measurements reveal that on a delivered surface area basis, large and small agglomerates of carboxylated IONPs have similar inherent potency for the generation of ROS, induction of stress-related genes and eventual cytotoxicity. The results suggest that reactive moieties on the agglomerate surface are more efficient in catalysing cellular ROS production than molecules buried within the agglomerate core. Because of the dynamic, size and density-dependent nature of ENP delivery to cells *in vitro*, the biological consequences of agglomeration are not discernible from static measures of exposure concentration (μg/ml) alone, highlighting the central importance of integrated physical characterisation and quantitative dosimetry for *in vitro* studies. The combined experimental and computational approach provides a

Correspondence: Brian D. Thrall, Biological Sciences Division, Center for Nanotoxicology, Pacific Northwest National Laboratory, Box 999, MS J4-02, Richland, WA 99352, USA. brian.thrall@pnnl.gov.

**Declaration of interest** The authors report no conflicts of interest. The authors alone are responsible for the content and writing of the paper.

Supplementary material available on online **Supplementary Figures S1–S3**.

quantitative framework for evaluating relationships between the biocompatibility of nanoparticles and their physical and chemical characteristics.

**Keywords**

nanotoxicology; agglomeration; iron oxide nanoparticles; oxidative stress; gene expression; dosimetry modelling

## Introduction

The incorporation of nanoscale materials into industrial technologies and consumer goods is a rapidly escalating global phenomenon. In parallel, there is a growing focus on the safety of the wide variety of engineered nanoparticles (ENPs) used in these applications, particularly with concern for inhalation as a route of potential occupational exposure in humans (Maynard et al. 2006; Li et al. 2010; Teeguarden et al. 2008; Warheit 2001). Because of the large diversity of nano-materials emerging for a growing range of applications, cellular-based (*in vitro*) assays play increasingly important roles in evaluating their potential hazards and for prioritisation of more costly (*in vivo*) toxicity testing. Frequently however, the physicochemical characteristics of ENPs differ dramatically in cell culture medium compared with their original formulation. In particular, high ionic strength, neutral pH and the presence of amino acids and other zwitterions in typical culture media alter the surface potential of ENPs, often resulting in spontaneous agglomeration. Serum proteins found in culture medium also adsorb to ENP surfaces, forming a protein corona that can further modulate the dispersion state of some ENPs (Bihari et al. 2008). These physical processes are highly dynamic and differences in the composition of the medium or serum can cause identical ENPs to form different sizes of agglomerates that bear distinct protein subsets (Maiorano et al. 2010; Lesniak et al. 2010). These complex and dynamic behaviours pose significant hurdles for specifying the structural features of ENPs that determine biocompatibility, and make it difficult to compare biological results across studies or different test systems.

The effective size and density of particles in cell culture systems are a function of their agglomerate state, packing density and shape. These properties can have profound impact on the rate of delivery to cells in culture by diffusion and gravitational settling (Teeguarden et al. 2007; Hinderliter et al. 2010). In addition, the mechanism and kinetics of cellular uptake of ENPs is influenced by both particle diameter and shape (reviewed in Albanese et al. 2012). Numerous studies have postulated nanoscale particles (<100 nm diameter) have inherently increased potential for toxicity compared with larger diameter particulates, due to their increased surface-to-mass ratio and greater proportion of surface-available chemically reactive groups (reviewed in Oberdorster et al. 2005). Because the physical processes governing agglomeration are difficult to control, few studies have compared biological responses across different size agglomerates of the same primary ENP. Recent *in vitro* studies have evaluated the cytotoxicity of ENPs whose agglomeration state was altered by dispersion in media containing different concentrations of serum protein (0–20%), different serum proteins (e.g. calf serum vs. bovine serum) or by varying the polymeric or surfactant

dispersants used to prepare the particles (Murdock et al. 2008; Mahmoudi et al. 2009; Kittler et al. 2010; Sager et al. 2007; Mahl et al. 2010). In approaches like these, the use of different proteins, serum levels or surface treatments precludes associating differences in cell uptake or response with differences in agglomerate size alone. Physical methods such as ultrasonication have also been used in attempt to disrupt and control agglomerate size (Murdock et al. 2008). However, ultrasonication is only weakly and transiently effective in disrupting agglomerates and can also cause oxidative modifications or otherwise damage the ENP and/or protein corona surface. Furthermore, an important shortcoming of these and other studies of ENP agglomeration (Zook et al. 2011; Karlsson et al. 2009; Park et al. 2008; Okuda-Shimazaki et al. 2010; Albanese & Chan 2011; Gosens et al. 2010) is that comparisons of the biological effects of different ENP preparations are typically based on measures of exposure concentration (μg/ml) rather than measured cellular dose of ENP. The dynamic, size and density-dependent nature of ENP delivery to cells *in vitro* by gravitational settling and diffusion can lead to significantly different cellular doses of these materials (Hinderliter et al. 2010; Teeguarden et al. 2007). In the absence of quantitative cell dosimetry measurements, it is not possible to determine if the differences in biological responses associated with agglomerated ENPs are a reflection of a change in physical property, a change in cellular dose or a combination of these factors.

In the present work, we investigated the influence of agglomeration state, surface modification and cellular delivery of iron oxide nanoparticles (IONPs) on the biological response of mouse lung alveolar type II (C10) epithelial cells. The main focus of this study was to determine the potential impacts that physical agglomeration can have on delivered cell dose and *in vitro* analysis of ENP biocompatibility. IONPs are widely used in biomedical applications such as imaging, and diagnostic applications in human, site-directed drug delivery and anticancer hyperthermia therapy (reviewed in Huber 2005). Due to their catalytic activities, IONPs are also used in the coal industry to produce clean fuels (Huber 2005) and may pose a risk for occupational exposure of humans by inhalation. It has been proposed that IONPs may cause toxicity through oxidative stress-mediated responses (reviewed in Singh et al. 2010). C10 cells were used as model alveolar type II epithelial cells, which play critical roles in the normal function of the lung by producing surfactants and regenerating type I epithelial cells (Weaver & Whitsett 1991). These cells effectively internalize particles ranging in diameter from nanometres to a few microns and participate in immune cell recruitment through the release of chemokines (Kato et al. 2003; Stringer et al. 1996; Ovrevik et al. 2006).

We developed a strategy to control IONP agglomerate size by altering the ionic concentration during stock particle suspension, followed by stabilising the formed agglomerates with a serum protein coating. Using IONPs with two surface modifications (carboxylated, aminated), this strategy was applied to create stable agglomerates with diameters ranging from 276 nm to 1.5 μm which have protein coronas from a common serum protein source and bear similar net zeta potentials in conventional culture medium. IONPs also provide a useful model nanoparticle which permitted us to directly quantify cell dose using a magnetic particle detection (MPD) system recently developed at their laboratory (Minard et al. 2012; Ferguson et al. 2011). MPD exploits an oscillating magnetic field together with the non-linear response of particle magnetisation to quantify

superparamagnetic particle mass in biological samples. In addition to sensitivity and signal stability over time, MPD has the important advantage of being sensitive to iron only when it is in particulate form. In addition to direct dosimetry measurements, the *In vitro* Sedimentation, Diffusion and Dosimetry (ISDD) (Hinderliter et al. 2010) model was used to aid in interpreting particle transport processes in cell culture. ISDD was developed from first principles of particle diffusion and sedimentation using multiple nanoparticle core types, including iron oxide. The results demonstrate that agglomeration can have a substantial effect on dose rate. Accounting for these dosimetry differences, the biological responses to small and large agglomerates are similar on a delivered surface area basis reinforcing the importance of relating responses to cellular doses for *in vitro* toxicity studies.

## Materials and methods

### Particle synthesis and characterisation

Superparamagnetic $Fe_3O_4$ nanoparticles were prepared by chemical co-precipitation method (Lu et al. 2007) at room temperature (23°C). Typically, 0.2M $FeCl_3$ (anhydrate, EM Science) and 0.1M $FeSO_4{\cdot}(a_2O$ (J. T. Baker) were mixed in 100 ml $H_2O$ under $N_2$. Then 10 ml of 29.5 wt% $NH_3$. $H_2O$ (J. T. Baker) was injected into the mixture with vigorous stirring. Upon adding the $NH_3.H_2O$, the colour of the mixture turned from brown to black immediately, implying formation of iron hydroxide. After stirring overnight for dehydration, the $Fe_3O_4$ colloidal nanoparticles were collected by a magnet, and washed with deionised $H_2O$ three times.

The $Fe_3O_4$ nanoparticles were further functionalised by grafting amine or carboxyl groups on the surface through covalent binding (see Supplemental Information, Figure S1). For surface modification with amines, the washed $Fe_3O_4$ nanoparticles were redispersed into a 250 ml mixture of ethanol and $H_2O$ (volume ratio 20:1) at pH ~8.5 adjusted by $NH_3.H_2O$, and then 2 ml of silane coupling agent, *N*(trimethoxysilylpropyl)ethylenediamine-triacetic acid-trisodium salt (35% in water, Gelest), was added drop by drop under stirring. After 12 h, the reaction mixture was adjusted to pH ~3.5 by HCl and reaction was allowed to continue for additional 12 h for completion. The functionalised $Fe_3O_4$ nanoparticles were collected by a magnet, and repeatedly washed by deionised $H_2O$ until near neutral pH. In the washing process, particles were redispersed by sonication and collected by magnet so that ionic and non-magnetic impurities were removed. At neutral pH, the amine groups were protonated as positively charged $-NH_3^+$ groups. For surface modification with carboxyl groups, the above processes were repeated using N(trimethoxysilylpropyl)ethylenediamine-triacetic acid-trisodium salt (35% in water, Gelest) as the silane coupling agent. Deionised $H_2O$ (resistance >18 MΩ·cm) was used throughout the experiments, and all reactions were performed under $N_2$ atmosphere or in closed containers to protect samples from oxidation. Images of the synthesised $Fe_3O_4$ nanoparticles were obtained by transmission electron microscope (TEM) (Zeiss, Libra 120) and scanning electron microscope (SEM) (Zeiss Merlin) measurements, and average primary particle size was determined by digital analysis of at least randomly chosen 200 particles. Average hydrodynamic sizes and zeta potentials were evaluated by dynamic light scattering (DLS) and zeta potentiometry (Brookhaven 90 Plus/ZetaPlus Analyzer).

## Agglomerate preparation and characterisation

The approach used to prepare controlled agglomerates is illustrated in Figure 1. The underlying rationale of the approach is to alter the ionic strength of the initial buffer. The stock particles are diluted to decrease repulsive charges and permit agglomeration to occur spontaneously, followed by addition of serum protein to stabilise the formed agglomerates. The stock solutions of agglomerates are then diluted in complete culture medium such that differences in ionic strength and protein concentration of the final cell treatment conditions are negligible. To create small agglomerates, a well-dispersed aqueous IONP stock solution (10 mg/ml) is pipetted into a tube containing equal volume of fetal bovine serum (FBS) and mixed by pipetting. Working particle dilutions are then prepared by adding this mixture into RPMI media containing 3% FBS. In this case, IONPs are stabilised by proteins in FBS before they agglomerate to large sizes resulting in smaller agglomerates. To create large agglomerates, the IONP stock solution is pipetted into an ionic solution (RPMI without FBS for amine-modified IONPs or 10× concentrated phosphate buffered saline (PBS) (1.37 M NaCl, 100 mM phosphate and 27 mM KCl) for carboxymodified IONPs), mixed by pipetting and allowed to agglomerate for 4 h. The ions in the salt solution neutralise the charge on the IONP surface causing them to agglomerate quickly. After the IONPs have agglomerated, FBS is added to prevent further agglomeration resulting in large, stable agglomerates. The typical v/v mixing ratio for IONP: ionic salt:FBS was 1:0.5:0.5.

Agglomerate size and zeta potential were measured with ZetaPALS Particle Sizing Software (Brookhaven Instruments Corp., Holtsville, NY, USA) using an aliquot of the particle solution used for cell exposure studies. Particle size was determined using average effective diameter ($n = 5$). Zeta potential values represent the average of at least 5 data points collected when the relative residual was <0.02.

## Cell culture

Stock cell cultures of the C10 mouse alveolar epithelial line were maintained in RPMI medium supplemented with 10% FBS, 2 mM L-glutamine, 100 U/ml penicillin and 0.1 mg/ml streptomycin in a humidified atmosphere of 5% $CO_2$–95% air at 37°C. For particle treatment experiments, cells were seeded in 6-well plates at $2.5 \times 10^5$ cells/well and allowed to attach overnight. Particle dilutions were added to cells in 2.5 ml of fresh media with serum and incubated at 37°C for the duration of the experiment. Unbound particles were removed by washing with PBS three times and the cells were harvested using 0.05% trypsin, centrifuged and resuspended in 100 μl PBS and analysed using MPD as described below. Cell viability was measured using alamarBlue reagent (Invitrogen, Carlsbad, CA, USA) and a fluorescence plate reader exactly as described by the manufacturer.

## Cellular IONP uptake measurement

The cellular content of IONP agglomerates was measured using a custom-built magnetic particle detector as described previously (Hinderliter et al. 2010; Minard et al. 2012). The detection system measures iron oxide associated with particles, but not dissolved iron species, which lack the superparamagnetic property required for detection. Serial dilutions of stock nanoparticle suspensions were used to generate a standard curve for IONP content. Standard curves were made in the appropriate biological matrix, for cell culture unexposed

cells. The measured cellular content of IONP was subsequently normalised to the number of cells per dish.

### Intracellular ROS measurement

The generation of intracellular reactive oxygen species (ROS) was monitored with peroxide-sensitive fluorescent probe, 2,7-dichlorodihydrofluorescein diacetate (CM-$H_2$DCFDA) (Sigma, St. Louis, MO, USA), according to the manufacture's guideline. Briefly, cells were washed with PBS, harvested with 0.05% trypsin, centrifuged, resuspended in 100 μl PBS and loaded with 10 μM CM-$H_2$DCFDA (excitation 492 nm/emission 517 nm) from a stock solution in dimethyl sulfoxide (DMSO). After a 30-min loading in a 37°C dark incubator, cells were washed again with PBS, resuspended in 400 μl PBS and analysed under the FL-1 channel using a flow cytometer (FACSAria, BD Biosciences, San Jose, CA, USA). At least 10,000 cells per treatment were analysed to assess the level of fluorescent intensity. FCS Express (De Novo Software, Los Angeles, CA, USA) was used to calculate median and mean intensities from fluorescence distributions.

### Real time quantitative RT-PCR

Expression of individual mRNAs was measured by real-time quantitative RT-PCR (qRT-PCR). Complementary DNA was synthesised from total RNA via reverse transcription using the QuantiTect kit (Qiagen, Valencia, CA, USA), which includes reagents for genomic DNA removal. To further ensure the specificity of the amplifications, primer pairs were designed to span introns. PCR reactions were carried out using Power SYBR Green Master Mix reagents according to the manufacturer's instructions (Applied Biosystems, Foster City, CA, USA) in an Applied Biosystems StepOnePlus cycler. Cycle parameters were: enzyme activation for 10 min at 95°C, followed by 45 cycles of denaturation at 95°C for 15 s and annealing/extension at 60°C for 60 s. Melting curve analyses were performed in each run. Relative expression was determined using the $\Delta\Delta C_T$ method with samples normalised to the expression level of the cyclophilin A transcript, the product of the mouse *Ppia* gene. All analyses were performed on individual samples from triplicate dishes of cells. The accession numbers and forward and reverse primer sequences for the genes analysed included: cyclooxygenase-2 (Cox-2) (NM_011198.3), F: 5′-gatgctcttccgagctgtg-3′, R: 5′-ggattggaacagcaaggattt-3′; heme oxygenase-1 (Hmox1) (NM_010442.2), F: 5′-aggctaagaccgccttcct-3′, R: 5′-tgtgttcctctgtcagcatca-3′; inducible nitric oxide synthase (iNOS) (NM_010927.3), F: 5′-ggagcctttagacctcaacaga-3′, R: 5′-aaggtgagctgaacgaggag-3′ and Fos-related antigen 1 (Fosl1) (NM_010235.2), F: 5′-ccgagactacggggaacc-3′, R: 5′-gcttggcacaaggtggaa-3′.

### Dosimetry modelling

The accumulation/delivery of IONP agglomerates associated with C10 epithelial cells during *in vitro* exposures was modelled using the ISDD model (Hinderliter et al. 2011), as previously described. The fraction of material delivered to cells that remained associated with cells was fitted to the experimental data, and was time dependent. The agglomerates were modelled with a fractal dimension (DF) of 2.0–2.4 and packing factor (PF) of 0.637 (Hinderliter et al. 2011). The particle diameter ($d$) was equal to the value reported by TEM (13 nm), and the agglomerates size ($d_{agg}$) were the values measured by DLS in the cell

culture media. The number of particles per agglomerate ($N_p$) was then calculated using the following equation as described by Sterling et al. (2005) after selecting a value for *DF* which gave the best fit between modelled and experimentally observed delivery.

$$N_p = PF\left(\frac{d_{agg}}{d}\right)^{DF}$$

Other model parameters were: temperature, 310°K; media density, 1.0 g/cm$^3$; media viscosity, 0.00074 Pa•s (reflecting the presence of serum proteins in the media) and an iron oxide particle density of 5.2 g/cm$^3$. The media volume was 2.5 ml and the media height was 2.6 mm.

## Results

### Characterisation of IONPs and their agglomerates

Aminated and carboxylated IONPs were generated from superparamagnetic $Fe_3O_4$ particles using silane precursors, as illustrated in Figure S1 provided in the Supplementary Information. Electron microscopy images of the IONPs are provided in Figure 2. The average diameter of the nanoparticles was 12.8 + 2.9 nm, with no discernible differences in size due to the surface functional groups as determined by TEM. High-resolution TEM analysis also confirmed the crystal structure of magnetite (Figure 2B). Zeta potential measurements conducted with the primary particles dispersed in deionised water confirmed that surface functionalisation of the IONPs significantly altered their net surface charge, with carboxylated and aminated IONPs having average net zeta potentials of −45 + 2 and +35 + 4 mV, respectively, compared with the unmodified IONP precursors (−33 mV). Hydrodynamic diameters of the primary carboxylated and aminated particles diluted in water were 56 + 7 and 238 + 22 nm, indicating that surface amination promoted greater agglomeration than did carboxylation. Because of their small size, the IONPs exhibited superparamagnetic properties (Huang et al. 2011) which were used later for quantification of their abundance.

IONPs tend to rapidly agglomerate in buffers or cell culture media due to presence of counter ions and charged amino acids/proteins which decrease the screening length of charged functional groups on the ENP surface. The physical propensity of the IONPs to agglomerate in liquid medium makes comparative experiments between monodispersed particles and agglomerates of the same material impracticable. Therefore, using the strategy illustrated in Figure 1, we took advantage of this property of IONPs to generate stable agglomerates of different effective diameters for comparison, while maintaining the final cell culture media constituents effectively constant. Table I summarises the effective diameters and zeta potential values of four agglomerate samples, two each generated from carboxylated- and amine-functionalised IONPs, after stabilisation with a protein corona. Small (C442S) and large (C442L) agglomerates of the carboxylated IONPs had hydrodynamic diameters of 276 and 689 nm, respectively, in cell culture media as measured by DLS. Similarly, small (A262S) and large (A262L) agglomerates of aminated IONPs had hydrodynamic diameters of 360 and 1463 nm, respectively (for corresponding DLS graphs see Supplementary Figure S2). Because each agglomerate type was stabilised by coating

with a common source of serum proteins, the resulting net zeta potentials for all particles were similarly negative in cell culture medium, with the amine-functionalised particles slightly more positive than the carboxylated particles (Table I).

## Impact of agglomeration on cellular dose and dose rate

IONPs agglomerates were incubated with C10 lung epithelial cells cultured as a monolayer, and the amount of IONP associated with cells (cellular dose) was quantified as a function of exposure concentration and time using a MPD system developed in our lab (Ferguson et al. 2011; Minard et al. 2012). An important advantage of this method of quantification is that the superparamagnetic properties detected by MPD rely on iron being in particulate form (Ferguson et al. 2011), allowing unambiguous measurements of intact IONP versus ionic forms of iron that are relatively abundant in biological systems. For all particles, the total cellular dose of IONPs after 4 h of exposure was linearly related to their mass concentration in media (Figure 3A and B), but their cellular dose rates were significantly different. The difference in slopes of the IONP mass cellular dose/concentration curve between the large and small agglomerates was 1.8 or 8 times for the carboxylated and aminated particles, respectively. A full time course of the rate of accumulation of each IONP at an exposure concentration of 10 μg/ml showed that the larger agglomerates accumulated more rapidly in cells than the smaller agglomerates (Figure 3C and D). During the first 4 h exposure, larger agglomerates of carboxylated IONPs accumulated at ~50% faster rate than smaller agglomerates, and accumulated mass differences of over fivefold were observed for aminemodified particles. These differences in the rate of increase in cellular dose could be the result of either differences in particle delivery, or particle uptake, or a mix of both. We used an available computational model (ISDD) to evaluate these alternatives and found that the rates of accumulation for the particles were consistent with differences in particle delivery to cells. It is important to point out that the terms ‘delivery’ and ‘cell-associated material’ refer to IONPs associated with the cells at the time of analysis, after washing to remove loosely bound particles. The material quantified by MPD may be membrane-bound or internalised within the cells. In this respect, MPD provides an overall lower bound measure of delivered dose, but a direct measure of cell-associated dose. Figure 3 also shows representative images of C10 cells treated with equal mass concentrations (10 μg/ml) of small or large agglomerates of either carboxylated (Figure 3E and F) or aminated (Figure 3G and H) particles for 4 h, where cells are stained with nuclear fast red and iron oxide is stained with Prussian blue. The significantly greater cellular dose achieved with larger agglomerated forms of the IONPs is also evident from the intense differences in staining.

## Cytotoxicity

Small and large agglomerates of carboxylated and aminated IONPs were incubated with C10 cells for 24 h using the same mass concentrations (μg/ml) as indicated in Figure 3A, and cell viability was assessed as described in the section “Materials and methods”. Agglomerates of carboxylated IONPs induced a dose-dependent inhibition in cell viability, with C442S being twice as cytotoxic on a cellular mass dose basis (C442S cell dose for 50% inhibition, $EC_{50}$ = 29 pg/cell; C442L, $EC_{50}$ = 58 pg/cell) (Figure 4A). Interestingly, cell viability measurements indicated that the agglomerates generated from IONPs with amine surface modifications were largely non-cytotoxic to C10 cells. After 24 h of exposure ~90% of the

cells remained viable after treatment with the aminated particles, even at cellular mass doses in the same range as those causing toxicity in cells treated with the carboxylated particles (Figure 4B).

## Expression of antioxidant and stress response genes

To investigate the impact of ENP agglomeration on oxidative stress-regulated responses in cells, pRT-PCR was used to measure mRNA levels of redox-regulated genes. For these experiments, mRNAs representative of several redox-regulated transcriptional pathways were measured to provide a general assessment of the oxidative stress transcriptional response in the cells, including the Nrf2 (Hmox1), nuclear factor-kappaB (NF-κB) (iNOS, Cox-2) and activator protein 1 (AP-1) (Fosl1) pathways. Consistent with the minimal cytotoxicity induced by A262S and A262L samples, we initially found that relatively high cellular doses of amine-modified IONPs failed to induce a biologically significant (>twofold) change in gene expression for these genes (see Supplementary Figure S3). Other antioxidant response genes analysed (Txnrd1, Gclc) were also not significantly altered by treatment with amine-modified IONPs (data not shown). By contrast, exposure to both sizes of carboxylated IONP agglomerates induced mRNA levels of Cox-2 (*aka* Ptgs2), iNOS, Fosl1 and Hmox1 in a cellular mass dose-dependent manner (Figure 5). The results also show that C442S induced a greater magnitude change in gene expression at lower total mass cellular doses compared with C442L. For example, cells treated with C442S showed a greater increase in iNOS mRNA compared with C442L at cell doses up to ~30 pg/cell. From 30 to 60 pg/cell there were minimal dose-dependent changes in iNOS expression for cells treated with C442L. Below cellular doses of ~5 pg/cell, no significant effects on gene expression were observed for either C442S or C442L treatments. A 2-factor ANOVA analysis of cellular dose–response profiles above this apparent threshold dose revealed that C442S induced a greater level of expression of Fosl1 ($p = 0.017$), iNOS ($p = 0.024$) and Txnrd1 ($p = 0.019$) compared with C442L, with a similar trend for Cox-2 ($p = 0.69$, non-significant). Thus, small agglomerates of carboxylated IONPs were more effective at inducing cellular stress responses compared with large agglomerates when compared at equivalent cellular mass doses of IONPs.

## Dosimetry modelling and delivered agglomerate surface area

The observed differences in cytotoxicity and gene expression induced by equivalent cellular mass doses of C442S or C442L could be a reflection of inherent changes in biological reactivity of the particles due to agglomeration state. Alternatively, if these cellular responses are initiated by reactive surface molecules on the agglomerates rather than total iron content, these differences might also be explained by differences in the available surface area of C442S and C442L delivered to cells. Our observations that surface modification of the IONPs results in very different cytotoxicity and stress gene induction responses, despite delivery of high mass levels of the IONPs, also supports the hypothesis that these cellular responses are initiated by surface reactive groups. We therefore investigated how the dose–response profiles for cytotoxicity and redox-sensitive gene regulation were compared for small and large agglomerates based on estimated available surface area cellular dose. These analyses focused on C442S or C442L, since the amine modified agglomerates were neither cytotoxic nor induced significant changes in redox-regulated mRNAs. Because agglomerates

are not necessarily composed of efficiently packed particles, and efficient experimental methods for measuring surface area of ENP agglomerates in cell culture systems are not available, the total delivered surface area of C442S and C442L was obtained by modelling, assuming a fractal structure as described by Sterling et al. (2005). We first used the ISDD model (Hinderliter et al. 2010) to derive boundaries for the DF of agglomerates. Transport of different agglomerates through liquid cell culture media was modelled using ISDD and benchmarked against the experimental data obtained from MPD measurements. To evaluate model behaviour against the experimental data, DF values for the IONP agglomerates were varied between 2.0 and 2.4, based on previously reported value of “around 2” for IONPs (Hinderliter et al. 2010). For this range of plausible values of DF, delivered iron oxide values calculated by ISSD were in close agreement with measured values of cell-associated iron oxide (Figure 6), differing at most by a factor of approximately 2. Of the values of DF tested, 2.0 and 2.2 provided the best fits against experimental results for C442S and C442L respectively, consistent with previous reports for metal oxide particles (Limbach et al. 2005; Hinderliter et al. 2010). Solving for the number of primary particles in each agglomerate using this DF and (Eq. 1), as described in the section “Materials and methods”, we calculated on an average 216 and 2889 single particles per agglomerate for C442S and C442L, respectively. The number of agglomerates delivered per cell was calculated by dividing the number particles in the measured mass of particles in the cells by the number of particles per agglomerate. The corresponding agglomerate surface area was calculated as the surface area of the sphere with the measured diameter of the agglomerate.

Figure 7 shows the experimentally measured cytotoxicity and redox-regulated gene expression responses of cells plotted as a function of the estimated surface area cellular dose of IONP agglomerates delivered to the cells. When normalised to the available surface area cellular dose, the C442S and C442L dose–response profiles for induction of oxidative stress responsive genes (4 h) and cytotoxicity (24 h) converged and the size-dependent differences in these responses observed on a mass cellular dose were less apparent. Flow cytometry analyses of the level of fluorescence in cells loaded with the redox-sensitive dye CM-$H_2$DCFDA were also conducted to provide a general estimate of oxidative stress. These results also indicate similar levels of ROS were induced in cells treated with equivalent surface area of C442S and C442L (Figure 7A).

To determine whether oxidative stress is indeed a central mechanism underlying the cytotoxicity of carboxylated IONP agglomerates, we also investigated whether pretreatment with the antioxidant N-acetylcysteine (NAC) modulated the cellular response to carboxylated IONPs. The results shown in Figure 8 demonstrate that pretreatment with NAC resulted in a dose-dependent inhibition of cytotoxicity induced by carboxylated IONPs. Nearly complete inhibition of cytotoxicity was achieved by pretreatment with 10 mM NAC. Although the data do not discern whether the inhibitory effects of NAC are primarily mediated through intra-cellular or extracellular mechanisms, the results validate a contributing role of oxidative stress in mediating adverse cellular responses to these IONPs.

## Discussion

With the rapid growth of nanotechnology, *in vitro* systems play an essential role in hazard analysis of engineered nanomaterials. However, determining the potential hazard of nanoparticles is not a simple matter of evaluating the cellular effects of individual particles alone. Agglomeration is a primary characteristic of ENPs in cell culture medium that is often poorly controlled in studies comparing particles of different sizes or composition. In the case of occupational exposure to ENPs by inhalation, a large fraction of ENPs may also be agglomerated by the time lung cell targets are reached. Thus, characterisation of the impacts of agglomeration state is a necessary element of effective nanotoxicology screening strategies (Oberdorster et al. 2005). We therefore developed an approach to compare biological potencies of different agglomeration states of the same primary ENPs, while controlling other important cell culture conditions (ionic strength, serum content) and particle characteristics (net charge, hydrodynamic diameter). With inclusion of cell dosimetry measurements and modelling, this study demonstrates that the dynamic nature of nanoparticle delivery to cells in culture and the associated agglomerate size dependencies are not captured by static measures of exposure that are independent of particle characteristics, such as mass concentration (μg/ml). By measuring cellular dose directly, and controlling agglomerate size, the results show that one key physical property of particles does not have a strong influence on oxidative stress induced gene transcription, ROS generation or cytotoxicity. The strategy was motivated by the observations that unprotected “bare” ENPs rapidly agglomerate in cell culture media due to interactions with charged amino acids and other counter ions, which neutralise the stabilising electrostatic forces on the IONP surface and allow van der Waals forces to drive spontaneous particle agglomeration (Derjaguin & Landau 1993). Spontaneous agglomeration was stopped when proteins (FBS) were introduced to form a corona, which stabilised the agglomerates. This approach provides a realistic representation of “naturally” occurring ENP agglomerates that are neither perfect spherical structures nor homogeneous individual particles. The results in producing stable agglomerates are in agreement with previous studies which employed weakly absorbing non-electrolytes or serum-free medium to modulate ENP surface charge and generate large agglomerates (Albanese & Chan 2011; Zook et al. 2011), or used bovine serum albumin (BSA) or serum protein coatings to minimise uncontrolled agglomeration (Gualtieri et al. 2011; Bihari et al. 2008; Wells et al. 2011). Importantly, the net zeta potentials of all agglomerates used in this study lie in a narrow range of −12.5 to −17.2 mV in culture media (Table I). Although the specific composition of serum protein adsorbed to IONPs was not determined adsorbed to the IONPs, which may vary with agglomerate size, this study results are in agreement with previous studies that show serum protein adsorption neutralises ENP surfaces toward a slight net negative charge (Limbach et al. 2005; Rezwan et al. 2004). The most abundant protein in FBS is albumin, which carries a negative charge (~20 elementary negative charges per molecule) at physiologic pH and likely contributes to the overall negative zeta potential (Rezwan et al. 2004). The similar zeta potential values for each agglomerate sample has implications for this study since large differences in net surface charge can be excluded as a confounding variable in the comparisons.

Previous studies have evaluated biological effects of different size agglomerates composed of the same primary ENPs by comparing their effects after dispersion in protein-free medium versus medium supplemented with either serum (up to 20%) or BSA (Kittler et al. 2010; Mahl et al. 2010; Murdock et al. 2008; Gualtieri et al. 2011). Gualtieri et al. (2011) reported agglomeration of silica ENPs was reduced by addition of albumin, and that agglomerated silica ENPs induced more potent inflammatory responses in BEAS-2B cells than non-agglomerated particles. Murdock et al. (2008) found that depending on the core particle chemistry, addition of serum can either mitigate or promote agglomeration, and that addition of serum can reduce the cytotoxicity of some metal oxide particles. However, in these and similar studies (Kittler et al. 2010; Drescher et al. 2011), it could not be ascertained whether the differential cell responses observed were due to agglomeration changes *per se* or other surface chemistry changes associated with protein adsorption. Furthermore, the absence of protein in medium can impart stress on cells, and addition of serum may exert independent cytoprotective effects through introduction of growth factors and other plasma proteins present. These extrinsic variables are controlled in this study such that direct comparisons among different size agglomerates of identical ENPs can be made using conventional cell culture conditions. The primary experimental variable altered in this approach is agglomerate size, since at the time of cell exposure all other culture conditions (ionic strength, FBS concentration) are equivalent.

An additional shortcoming of previous studies of ENP agglomeration is that changes in cellular dose rate due to physical property changes caused by agglomeration are often not accounted for; making it difficult to draw firm conclusions about dose–response relationships. Cellular dose is a direct function of how the physical properties of a material are influenced by gravitation, diffusion and convection forces that dictate material transport (Teeguarden et al. 2007). Thus, quantification of cell-associated dose is essential for interpreting results from comparative studies involving different ENP entities (such as different material core chemistries, surface properties or agglomerate size) whose dose rates may differ significantly. The proper attribution of physical or chemical characteristics of nanoparticles to specific biological effects therefore requires careful consideration of the cellular dose. MPD provided a reliable method to quantify the total amount of IONP bound and internalised in cells, since the MPD sensor mechanism is sensitive to magnetisation signals from iron only when it is bound in particulate form (Ferguson et al. 2011; Minard et al. 2012). Our recent work has shown that MPD is sufficiently sensitive to quantify ~100 ng of superparamagnetic IONPs, and can even discriminate differences in rates of total cell binding/uptake of IONPs due to expression of specific endocytic receptors (Minard et al. 2012). Total cell-associated IONPs reached an asymptote during the 24 h exposure, which could either represent reduced delivery (depletion of media IONPs), saturation of binding/uptake mechanisms or a combination of these factors. Simulations of the MPD data using ISDD (Figure 6) suggest that reduced delivery due to depletion of IONPs in the media accounted for at least part of the asymptotic behaviour. Regardless of the underlying mechanism of cell interaction, by directly quantifying the dose of material delivered to the cells significant agglomeration-mediated differences in dose rate and total mass cellular dose become apparent, which were not evident based on media IONP concentration alone (Figure 3). The range of agglomerate diameters used in this study are representative of the extent of

spontaneous agglomeration that often occurs for many metal oxide ENPs in common cell culture medium formulations, as determined by DLS (Murdock et al. 2008). Under these commonly employed conditions, we found that the dose rate during the first few hours of cell exposure could vary by more than fivefold, and in extreme cases (A262L, Figure 3) total cellular dose could vary by >10-fold due to agglomeration state alone.

Similar observations were made in a recent study by Cohen et al. (2012), who used the ISDD model to determine the effect of different media dispersion protocols on nanoparticle agglomeration and dose deposition in cell culture. Both their study and this study results regarding delivered agglomerate surface areas are bounded by model estimates of the effective densities of agglomerates, a particle-specific function of the DF. Cohen et al. (2012) modelled agglomerate mobilities using ISDD, and reported that the effective density of agglomerates was relatively insensitive to changes in DF values. This study further incorporated direct measures of particle transport from MPD analysis, which coupled with size data, allowed us to infer effective density (vis-à-vis the DF). The empirical measurements of particle transport were consistent with different size agglomerates having similar effective densities. Although analytical methods to determine effective densities of nanomaterials are emerging (Wohlleben, 2012), the instrumentation for these approaches is not always widely available. It is noteworthy that we previously calculated the effective density of other iron oxide particles in cell culture medium and arrived at values that were almost identical to the results of this study (Hinderliter et al. 2010). While direct measurement of effective agglomerate densities may improve the approach, these observations provide additional confidence that the uncertainty in the calculations is small, supporting the premise that the effective density of the IONP agglomerates is relative constant across different agglomerate sizes.

Oxidative stress constitutes one of the primary mechanisms by which metal oxide nanoparticles have been shown to cause adverse biological effects (Xia et al. 2006; Zhang et al. 2012; Singh et al. 2010). Although iron oxides (magnetite and maghemite) particles are often regarded as low solubility, low toxicity materials, there are an ample number of contradicting reports in the literature regarding the potency of various IONPs to induce oxidative stress and cytotoxicity (Stroh et al. 2004; Mahmoudi et al. 2012, 2011; Brunner et al. 2006; Apopa et al. 2009; Zhang et al. 2012; Veranth et al. 2007; Singh et al. 2010). This study supports the conclusion that oxidative stress plays a central role in the biological activity of carboxylated IONPs, since the cytotoxic effects of these particles was strongly inhibited by NAC. Although agglomerates prepared from carboxylated IONPs caused significant stress gene induction and cytotoxicity, equivalent mass cellular doses of IONPs bearing amine surface modifications were relatively inert for these end points. In experiments using bone-marrow-derived macrophages, we have observed a similar pattern of enhanced activity of carboxylated IONPs, and found amine-modified IONPs more closely reflect the biocompatibility of unmodified iron oxide (Kodali et al. manuscript in preparation). These observations suggest that in the absence of surface carboxyl groups, IONPs are not cytotoxic until relatively high cellular dose levels (>75 pg/cell) are achieved. The results differ from a previous study that reported superparamagnetic IONPs tethered with amine functional groups caused greater cytotoxicity than when functionalised with carboxyl groups, when compared on a molar basis (Mahmoudi et al. 2011). Although

surface charges of the particles used in their study varied significantly, the extent of agglomeration is uncertain since size measurements were only reported for particles dispersed in water. By contrast, the low biological activity of aminemodified IONPs observed in this study is consistent with other studies that indicate IONPs are not cytotoxic up to high exposure concentrations in bronchial epithelial cells (Zhang et al. 2012; Veranth et al. 2007) or that aminemodified IONPs induce less cytotoxicity compared with carboxyl-modified IONPs in A3 human T lymphocytes (Ying & Hwang, 2010). Given the findings that effective cellular dose rates vary substantially among different IONP types in culture medium, sorting out the extent that conflicting reports reflect true differences in material chemistry or cell-type specific responses (Brunner et al. 2006) is challenging in the absence of corresponding dosimetry.

If one assumes that the cellular effects of IONPs are driven by the total mass amount of iron within an agglomerate, potentially via Fenton chemistry, the results suggest that small agglomerates of carboxylated IONPs induce oxidative stress more efficiently than larger agglomerates composed of the same primary particles. A biophysical explanation for such a change in the inherent bioreactivity of iron oxide due to physical agglomeration is not obvious. Available thermodynamic data indicate that at neutral pH ranges typical of cell culture conditions, iron oxides are generally of very low solubility (Schwertmann 1991). The MPD measurements also indicate the magnetisation properties of the IONPs were very stable over time frames of several weeks, further supporting minimal dissolution of the particles in liquid environments. Therefore, we hypothesised that the degree of oxidative stress is a function of solvent accessible surface area, and used dosimetry modelling in conjunction with experimental results to estimate the effective surface area cellular dose for the carboxylated IONP agglomerates. The results show that large and small agglomerates of carboxylated IONPs display a similar inherent surface area relationship for the generation of ROS, induction of oxidative stress-related genes and eventual induction of cytotoxicity. In conjuction with the strong correlations observed between cellular ROS levels and early mRNA induction of ROS-regulated genes (Figure 7), the results support the concept that reactive moieties on the particle surface are more efficient in catalysing cellular ROS production than molecules buried within the agglomerate core, the latter of which are expected to have reduced solvent accessibility. This hypothesis is supported by recent spin-trapping electron paramagnetic resonance experiments that demonstrate IONPs catalyse hydroxyl radical production via Fenton chemistry more efficiently at catalytic centres on the nanoparticle surface, as compared with dissolved metal ions (Voinov et al. 2011). Furthermore, adsorption of albumin on the IONP surface had little impact on its redox catalytic activity (Voinov et al. 2011). Thus, while IONP agglomerates do not necessarily behave simply as geometrically larger particles, they appear to retain the surface-dependent properties of primary particles to stimulate ROS. Future studies aimed at determining how carboxyl and other surface functional groups modulate this catalytic activity are warranted, given the trend toward design of multifunctional IONPs for medical imaging and diagnostics.

Appropriate physicochemical characterisation of ENPs and choice of dose metrics are common issues for *in vitro* nanotoxicology studies, compounded by limited knowledge about which physical and chemical characteristics of ENPs are most important for initiating

biological responses. Foremost, it is clear that relationships between particle characteristics and biological responses will be far more difficult to discover if their impacts on cellular dose and dose rates are not accounted for. In absence of this, commonly employed experimental paradigms based on exposure–response relationships alone are insufficient for understanding the properties of nanomaterials that dictate biocompatibility.

## Supplementary Material

Refer to Web version on PubMed Central for supplementary material.

## Acknowledgements

Support for this research was provided by Battelle Memorial Institute under a cooperative research and development agreement (#PNNL 2119) and by the National Institutes of Health grant U19 ES019544. Pacific Northwest National Laboratory is operated by Battelle for the US Department of Energy under contract ACO6 76RLO 1830. The authors also thank Dr. Libor Kovarik for technical support with TEM images conducted at the Environmental Molecular Sciences Laboratory, a DOE-funded National User Facility at PNNL.

## References

Albanese A, Chan WC. Effect of gold nanoparticle aggregation on cell uptake and toxicity. ACS Nano. 2011; 5:5478–5489. [PubMed: 21692495]

Albanese A, Tang PS, Chan WC. The effect of nanoparticle size, shape, and surface chemistry on biological systems. Annu Rev Biomed Eng. 2012; 14:1–16. [PubMed: 22524388]

Apopa PL, Qian Y, Shao R, Guo NL, Schwegler-Berry D, Pacurari M, et al. Iron oxide nanoparticles induce human microvascular endothelial cell permeability through reactive oxygen species production and microtubule remodeling. Part Fibre Toxicol. 2009; 6:1. [PubMed: 19134195]

Bihari P, Vippola M, Schultes S, Praetner M, Khandoga AG, Reichel CA, et al. Optimized dispersion of nanoparticles for biological in vitro and in vivo studies. Part Fibre Toxicol. 2008; 5:14. [PubMed: 18990217]

Brunner TJ, Wick P, Manser P, Spohn P, Grass RN, Limbach LK, et al. In vitro cytotoxicity of oxide nanoparticles: comparison to asbestos, silica, and the effect of particle solubility. Environ Sci Technol. 2006; 40:4374–4381. [PubMed: 16903273]

Cohen J, Deloid G, Pyrgiotakis G, Demokritou P. Interactions of engineered nanomaterials in physiological media and implications for in vitro dosimetry. Nanotoxicology. 2012; 7:417–431. [PubMed: 22393878]

Derjaguin B, Landau L. Theory of the stability of strongly charged lyophobic sols and of the adhesion of strongly charged particles in solutions of electrolytes. Prog Surf Sci. 1993; 43:30–59.

Drescher D, Orts-Gil G, Laube G, Natte K, Veh RW, Osterle W, et al. Toxicity of amorphous silica nanoparticles on eukaryotic cell model is determined by particle agglomeration and serum protein adsorption effects. Anal Bioanal Chem. 2011; 400:1367–1373. [PubMed: 21479547]

Ferguson RM, Minard KR, Khandhar AP, Krishnan KM. Optimizing magnetite nanoparticles for mass sensitivity in magnetic particle imaging. Med Phys. 2011; 38:1619–1626. [PubMed: 21520874]

Gosens I, Post JA, De LA Fonteyne LJ, Jansen EH, Geus JW, Cassee FR, et al. Impact of agglomeration state of nanoand submicron sized gold particles on pulmonary inflammation. Part Fibre Toxicol. 2010; 7:37. [PubMed: 21126342]

Gualtieri M, Skuland T, Iversen TG, Lag M, Schwarze P, Bilanicova D, et al. Importance of agglomeration state and exposure conditions for uptake and pro-inflammatory responses to amorphous silica nanoparticles in bronchial epithelial cells. Nanotoxicology. 2011; 6:700–712. [PubMed: 21793771]

Hinderliter PM, Minard KR, Orr G, Chrisler WB, Thrall BD, Pounds JG, et al. ISDD: A computational model of particle sedimentation, diffusion and target cell dosimetry for in vitro toxicity studies. Part Fibre Toxicol. 2010; 7:36. [PubMed: 21118529]

Hinderliter PM, Price PS, Bartels MJ, Timchalk C, Poet TS. Development of a source-to-outcome model for dietary exposures to insecticide residues: an example using chlorpyrifos. Regul Toxicol Pharmacol. 2011; 61:82–92. [PubMed: 21722690]

Huang HC, Barua S, Sharma G, Dey SK, Rege K. Inorganic nanoparticles for cancer imaging and therapy. J Control Release. 2011; 155:344–357. [PubMed: 21723891]

Huber DL. Synthesis, properties, and applications of iron nano-particles. Small. 2005; 1:482–501. [PubMed: 17193474]

Karlsson HL, Gustafsson J, Cronholm P, Moller L. Size-dependent toxicity of metal oxide particles–a comparison between nanoand micrometer size. Toxicol Lett. 2009; 188:112–118. [PubMed: 19446243]

Kato T, Yashiro T, Murata Y, Herbert DC, Oshikawa K, Bando M, et al. Evidence that exogenous substances can be phagocytized by alveolar epithelial cells and transported into blood capillaries. Cell Tissue Res. 2003; 311:47–51. [PubMed: 12483283]

Kittler S, Greulich C, Gebauer JS, Diendorf J, Treuel L, Ruiz L, et al. The influence of proteins on the dispersability and cell-biological activity of silver nanoparticles. J Mater Chem. 2010; 20:512–518.

Lesniak A, Campbell A, Monopoli MP, Lynch I, Salvati A, Dawson KA. Serum heat inactivation affects protein corona composition and nanoparticle uptake. Biomaterials. 2010; 31:9511–9518. [PubMed: 21059466]

Li JJ, Muralikrishnan S, Ng CT, Yung LY, Bay BH. Nanoparticle-induced pulmonary toxicity. Exp Biol Med. 2010; 235:1025–1033.

Limbach LK, Li Y, Grass RN, Brunner TJ, Hintermann MA, Muller M, et al. Oxide nanoparticle uptake in human lung fibroblasts: effects of particle size, agglomeration, and diffusion at low concentrations. Environ Sci Technol. 2005; 39:9370–9376. [PubMed: 16382966]

Lu AH, Salabas EL, Schuth F. Magnetic nanoparticles: synthesis, protection, functionalization, and application. Angew Chem Int Ed Engl. 2007; 46:1222–1244. [PubMed: 17278160]

Mahl D, Greulich C, Meyer-Zaika W, Koller M, Epple M. Gold nanoparticles: dispersability in biological media and cell-biological effect. J Mater Chem. 2010; 20:6176–6181.

Mahmoudi M, Hofmann H, Rothen-Rutishauser B, Petri-Fink A. Assessing the in vitro and in vivo toxicity of superparamagnetic iron oxide nanoparticles. Chem Rev. 2012; 112:2323–2338. [PubMed: 22216932]

Mahmoudi M, Laurent S, Shokrgozar MA, Hosseinkhani M. Toxicity evaluations of superparamagnetic iron oxide nanoparticles: cell “vision” versus physicochemical properties of nanoparticles. ACS Nano. 2011; 5:7263–7276. [PubMed: 21838310]

Mahmoudi M, Simchi A, Imani M, Milani AS, Stroeve P. An in vitro study of bare and poly(ethylene glycol)-co-fumarate-coated superparamagnetic iron oxide nanoparticles: a new toxicity identification procedure. Nanotechnology. 2009; 20:225104. [PubMed: 19433870]

Maiorano G, Sabella S, Sorce B, Brunetti V, Malvindi MA, Cingolani R, et al. Effects of cell culture media on the dynamic formation of protein-nanoparticle complexes and influence on the cellular response. ACS Nano. 2010; 4:7481–7491. [PubMed: 21082814]

Maynard AD, Aitken RJ, Butz T, Colvin V, Donaldson K, Oberdorster G, et al. Safe handling of nanotechnology. Nature. 2006; 444:267–269. [PubMed: 17108940]

Minard KR, Littke MH, Wang W, Xiong Y, Teeguarden JG, Thrall BD. Magnetic particle detection (MPD) for in-vitro dosimetry. Biosens Bioelectron. 2012; 43:88–93. [PubMed: 23287653]

Murdock RC, Braydich-Stolle L, Schrand AM, Schlager JJ, Hussain SM. Characterization of nanomaterial dispersion in solution prior to in vitro exposure using dynamic light scattering technique. Toxicol Sci. 2008; 101:239–253. [PubMed: 17872897]

Oberdorster G, Maynard A, Donaldson K, Castranova V, Fitzpatrick J, Ausman K, et al. Principles for characterizing the potential human health effects from exposure to nanomaterials: elements of a screening strategy. Part Fibre Toxicol. 2005; 2:8. [PubMed: 16209704]

Okuda-Shimazaki J, Takaku S, Kanehira K, Sonezaki S, Taniguchi A. Effects of titanium dioxide nanoparticle aggregate size on gene expression. Int J Mol Sci. 2010; 11:2383–2392. [PubMed: 20640159]

Ovrevik J, Refsnes M, Namork E, Becher R, Sandnes D, Schwarze PE, et al. Mechanisms of silica-induced IL-8 release from A549 cells: initial kinase-activation does not require EGFR activation or particle uptake. Toxicology. 2006; 227:105–116. [PubMed: 16963169]

Park EJ, Choi J, Park YK, Park K. Oxidative stress induced by cerium oxide nanoparticles in cultured BEAS-2B cells. Toxicology. 2008; 245:90–100. [PubMed: 18243471]

Rezwan K, Meier LP, Rezwan M, Voros J, Textor M, Gauckler LJ. Bovine serum albumin adsorption onto colloidal Al2O3 particles: a new model based on zeta potential and UV-vis measurements. Langmuir. 2004; 20:10055–10061. [PubMed: 15518493]

Sager TM, Porter DW, Robinson VA, Lindsley WG, Schwegler-Berry DE, Castranova V. Improved method to disperse nano-particles for in vitro and in vivo investigation of toxicity. Nanotoxicology. 2007; 1:118–119.

Schwertmann U. Solubility and dissolution of iron oxides. Plant Soil. 1991; 130:1–25.

Singh N, Jenkins GJ, Asadi R, Doak SH. Potential toxicity of superparamagnetic iron oxide nanoparticles (SPION). Nano Rev. 2010; 1:10.

Sterling MC JR, Bonner JS, Ernest AN, Page CA, Autenrieth RL. Application of fractal flocculation and vertical transport model to aquatic sol-sediment systems. Water Res. 2005; 39:1818–1830. [PubMed: 15899280]

Stringer B, Imrich A, Kobzik L. Lung epithelial cell (A549) interaction with unopsonized environmental particulates: quantitation of particle-specific binding and IL-8 production. Exp Lung Res. 1996; 22:495–508. [PubMed: 8886755]

Stroh A, Zimmer C, Gutzeit C, Jakstadt M, Marschinke F, Jung T, et al. Iron oxide particles for molecular magnetic resonance imaging cause transient oxidative stress in rat macrophages. Free Radic Biol Med. 2004; 36:976–984. [PubMed: 15059638]

Teeguarden J, Gupta A, Escobar P, Jackson M. Toxicology steps up to nanotechnology safety. RD Magazine. 2008; 50:28–29.

Teeguarden JG, Hinderliter PM, Orr G, Thrall BD, Pounds JG. Particokinetics in vitro: dosimetry considerations for in vitro nano-particle toxicity assessments. Toxicol Sci. 2007; 95:300–312. [PubMed: 17098817]

Veranth JM, Kaser EG, Veranth MM, Koch M, Yost GS. Cytokine responses of human lung cells (BEAS-2B) treated with micron-sized and nanoparticles of metal oxides compared to soil dusts. Part Fibre Toxicol. 2007; 4:2. [PubMed: 17326846]

Voinov MA, Sosa Pagan JO, Morrison E, Smirnova TI, Smirnov AI. Surface-mediated production of hydroxyl radicals as a mechanism of iron oxide nanoparticle biotoxicity. J Am Chem Soc. 2011; 133:35–41. [PubMed: 21141957]

Warheit DB. Inhaled amorphous silica particulates: what do we know about their toxicological profiles? J Environ Pathol Toxicol Oncol. 2001; 20(Suppl 1):133–141.

Weaver TE, Whitsett JA. Function and regulation of expression of pulmonary surfactant-associated proteins. Biochem J. 1991; 273(Pt 2):249–264. [PubMed: 1991023]

Wells MA, Abid A, Kennedy IM, Barakat AI. Serum proteins prevent aggregation of $Fe_2O_3$ and ZnO nanoparticles. Nanotoxicology. 2011; 6:837–846. [PubMed: 22149273]

Wohlleben W. Validity range of centrifuges for the regulation of nanomaterials: from classification to as-tested coronas. J Nanopart Res. 2012; 14:1300. [PubMed: 23239934]

Xia T, Kovochich M, Brant J, Hotze M, Sempf J, Oberley T, et al. Comparison of the abilities of ambient and manufactured nano-particles to induce cellular toxicity according to an oxidative stress paradigm. Nano Lett. 2006; 6:1794–1807. [PubMed: 16895376]

Ying E, Hwang HM. In vitro evaluation of the cytotoxicity of iron oxide nanoparticles with different coatings and different sizes in A3 human T lymphocytes. Sci Total Environ. 2010; 408:4475–4481. [PubMed: 20673962]

Zhang H, Ji Z, Xia T, Meng H, Low-Kam C, Liu R, et al. Use of metal oxide nanoparticle band gap to develop a predictive paradigm for oxidative stress and acute pulmonary inflammation. ACS Nano. 2012; 6:4349–4368. [PubMed: 22502734]

Zook JM, Maccuspie RI, Locascio LE, Halter MD, Elliott JT. Stable nanoparticle aggregates/agglomerates of different sizes and the effect of their size on hemolytic cytotoxicity. Nanotoxicology. 2011; 5:517–530. [PubMed: 21142841]

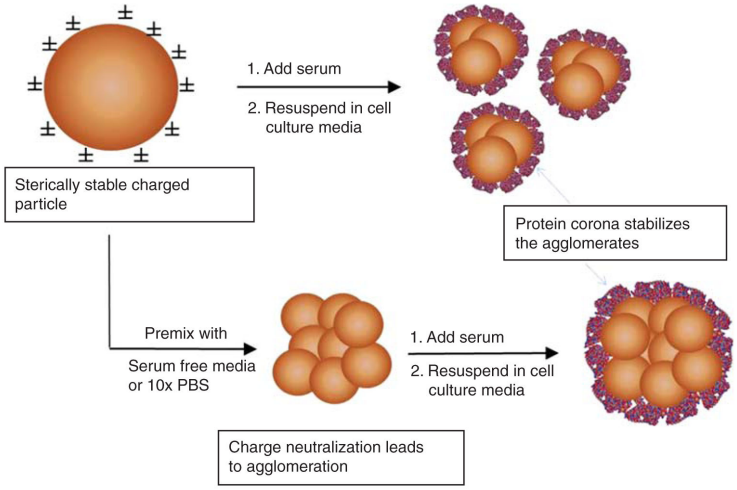


**Figure 1.**

Strategy used for preparing stabilised IONP agglomerates. Premixing stock IONPs in a small volume of fetal bovine serum (FBS) forms a protein corona on the IONP surface which sterically stabilises small agglomerates prior to dilution in cell culture medium. Larger diameter agglomerates were formed in a controlled fashion by premixing the IONPs in a small volume of either serum-free medium (amine-modified IONPs) or 10× PBS solution (carboxylated IONPs). The buffering capacity of serum-free medium and/or PBS leads to charge neutralisation and agglomeration. Agglomeration is stopped by stabilisation with FBS prior to dilution in complete medium.

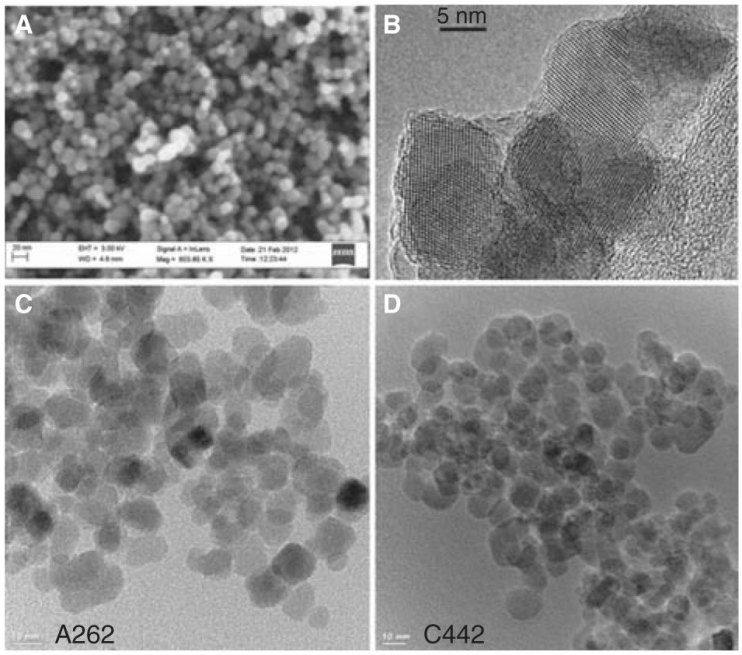


**Figure 2.**

SEM (A) and TEM (B–D) images of synthesised IONPs with average particle diameter of 12.8 nm. The high resolution TEM image in panel b highlights the crystallinity of the IONPs. Lower panels show TEM images of the amine (C) and carboxyl (D) surface-modified particles used in the cell studies.

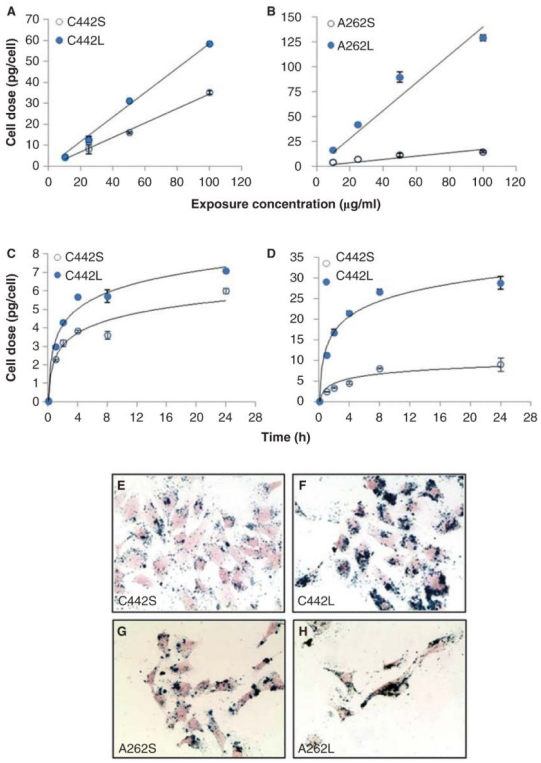


**Figure 3.**

Exposure- and time-dependent delivery of IONP agglomerates to cultured mouse C10 lung epithelial cells. Cells were treated with the indicated media concentrations of carboxylated (A) or amine-modified (B) IONPs for 4 h and total cell-associated IONPs were determined by magnetic particle detection, as described in the section “Materials and methods”. Solid lines represent a linear fit to the data (C442S, $y = 0.3447x$, $R^2 = 0.9942$; C442L: $y = 0.5865x$, $R^2 = 0.994$; A262S, $y = 0.1682x$, $R^2 = 0.9357$; A262L: $y = 1.4064x$, $R^2 = 0.9267$). The temporal patterns of cell association of carboxylated (C) and amine-modified (D) IONPs was determined after exposure to 10 μg/ml concentration and measured at the times indicated. Solid lines represent a logarithmic fit to the data (C442S, $R^2 = 0.9503$; C442L, $R^2 = 0.9811$; A262S, $R^2 = 0.9002$; A262L, $R^2 = 0.9788$). Panels E–H: Representative images of C10 cells after 4 h exposure to 10 μg/ml of small and large agglomerates of carboxylated IONPs (panels E, F) or aminated IONPS (panels G, H). Iron oxide is stained with Prussian blue and cells are stained with Nuclear Fast Red.

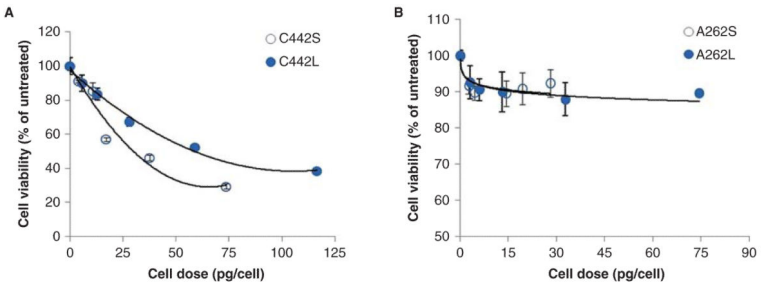


**Figure 4.**

Cytotoxicity dose–response profiles for C10 cells treated with small and large agglomerates of IONPs. Cytotoxicity was measured 24 h after exposure to agglomerates of carboxylated (A) or amine-modified IONPs (B). Cell dose values on the X-axis were determined by MPD, as described in the section “Materials and methods”. Exposure concentrations (μg/ml) for these dose equivalents were 5, 10, 50, 100 and 200 μg/ml (carboxylated) and 5, 10, 25, 50 and 100 μg/ml (aminated). On an absolute mass dose basis, C442S were found to be more cytotoxic compared with C442L. Values are mean + s.d. of at least triplicate biological replicates. Solid lines represent the best-fit regression model (polynomial or logarithmic) to the data (C442S, $R^2$ = 0.9548; C442L, $R^2$ = 0.9917; A262S, $R^2$ = 0.7141; A262L, $R^2$ = 0.9103).

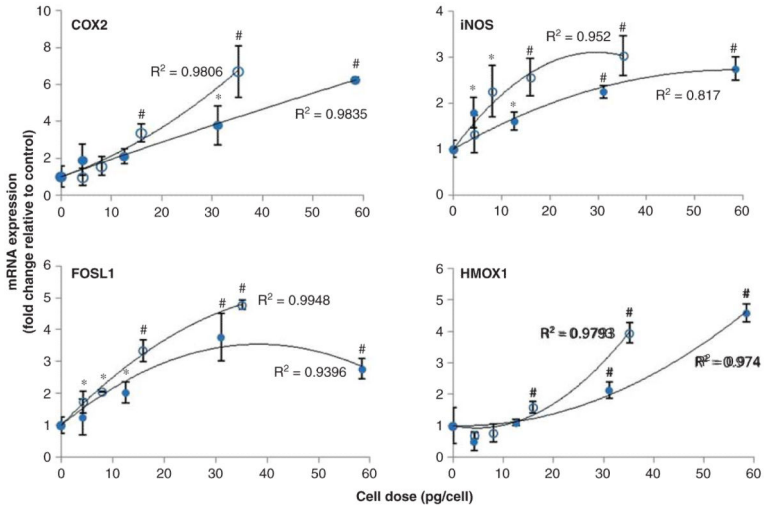


**Figure 5.**

Dose–response profiles for stress-related gene induction. Expression of genes associated with oxidative stress response pathways were determined by qRT-PCR after 4 h exposure of cells to varying concentrations of C442S (○) and C442L (•) agglomerates of carboxylated IONPs. The change in mRNA levels relative to untreated controls is shown as a function of mass cell dose, as determined by magnetic particle detection. Exposure concentrations (μg/ml) for these dose equivalents were 10, 25, 50 and 100 μg/ml. Solid lines represent a second order polynomial fit to the data. $^{*}p < 0.05$, $^{\#}p < 0.01$ compared with untreated control.

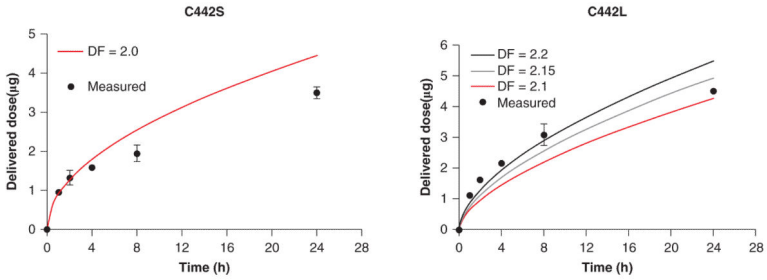


**Figure 6.**

Simulated transport of IONPs in culture medium. Shown is a comparison of the modelled and experimentally measured transport kinetics of small and large agglomerates of carboxylated IONPs. Particle transport was modelled for plausible values of the fractal dimension (DF); a DF of 2.0 and 2.2 provided the best correspondence between modelled and measured data for C442S and C442L, respectively.

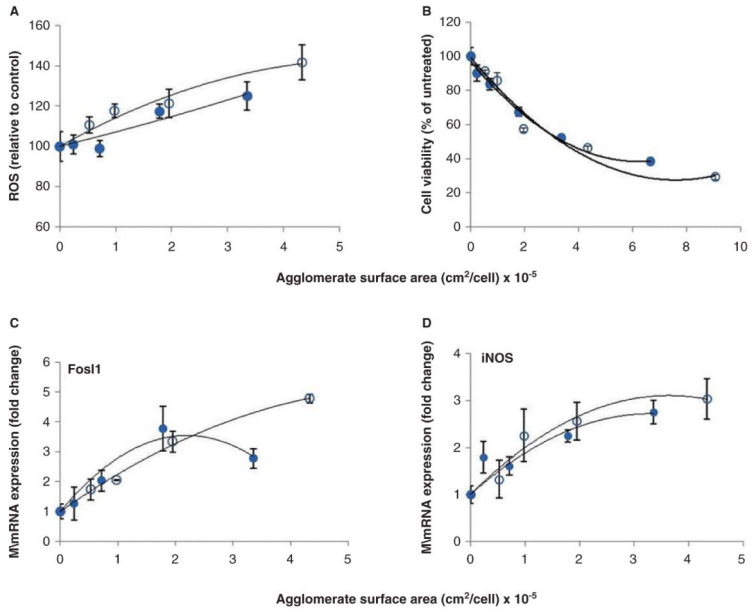


**Figure 7.**

Dose–response profiles for IONP agglomerates based on cellular surface area dose. Agglomerate surface area was calculated using fractal dimension (DF) values for agglomerates as identified from simulations. On a surface area metric basis, C442S (○) and C442L (•) caused equivalent levels of oxidative stress (A), cytotoxicity (B) measured at 24 h, and stress gene induction (C, D) measured at 4 h. Solid lines represent a second order polynomial fit to the data.

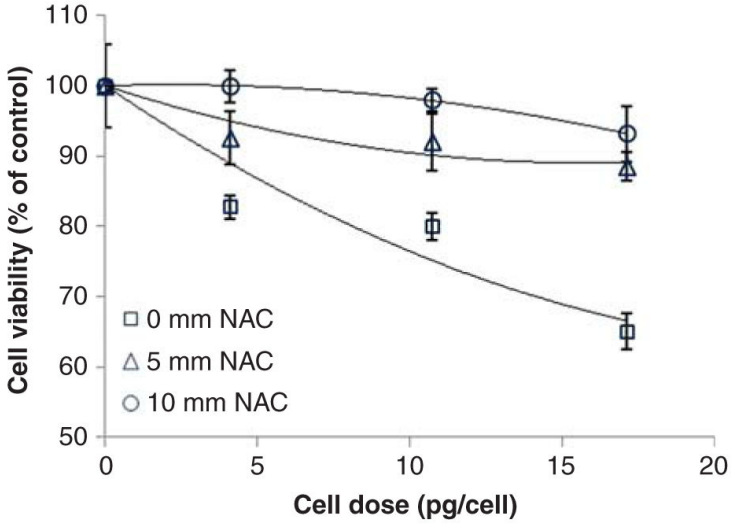


**Figure 8.**

*N*-Acetylcysteine protects C10 cells from carboxylated IONP cytotoxicity. C10 were pretreated for 24 h with the indicated concentrations of NAC followed by exposure for 24 h to small carboxylated IONPs. Cell viability was determined as described in the section "Materials and methods". Exposure concentrations (μg/ml) for these dose equivalents were 10, 25, 50 and 100 μg/ml. Values are mean + s.d. of a minimum of triplicate biological replicates. Solid lines represent a second order polynomial fit to the data.

**Table I**

Physical properties of IONP agglomerates.

| | | | | Zeta potential (mV) | |
|---|---|---|---|---|---|
| **Particle type** | **Nomenclature** | **Diameter (nm)** | **Polydispersity** | **Water** | **Culture media** |
| Carboxyl- small | C442S | 276 ± 6 | 0.254 | −37.6 ± 3.4 | −17.2 ± 2.3 |
| Carboxyl- large | C442L | 689 ± 43 | 0.250 | −32.6 ± 1.0 | −17.3 ± 2.0 |
| Amine- small | A262S | 360 ± 15 | 0.204 | −32.5 ± 0.7 | −15.2 ± 1.9 |
| Amine- large | A262L | 1463 ± 93 | 0.261 | −28.6 ± 3.8 | −12.5 ± 2.9 |

IONP, iron oxide nanoparticle.